SCIENTIFIC REPORTS

OPEN

Imaging Monitoring of Kupffer Cell Function and Hepatic Oxygen Saturation in Preneoplastic Changes During Cholangiocarcinogenesis

Seunghyun Lee[1], Jung Hoon Kim[1,2], Jeong Hwa Lee[2], Yoh Zen[3] & Joon Koo Han[1,2]

We investigated serial changes of the Kupffer cell (KC) function and hepatic oxygen saturation (sO_2) using contrast-enhanced ultrasound imaging (CEUS) and photoacoustic imaging (PAI) in preneoplastic changes during cholangiocarcinogenesis induced by obstructive cholangitis and N-nitrosodimethylamine in a mouse model. The CEUS and PAI were performed to assess Sonazoid contrast agent uptake by KC and changes in the sO_2 of liver parenchyma. An extensive bile ductular reaction, cystic dilatation, and epithelial hyperplasia with dysplastic changes were noted in the experimental group. During the preneoplastic changes, the parenchymal echogenicity on the Kupffer-phase of CEUS was continuously decreased in the experimental group, and which means that the Sonazoid phagocytosis by KC was decreased. The number of KCs was increased in the CD68 analysis, indicating functionally impaired KCs. There was a simultaneous serial decrease in sO_2 on PAI measurement of the experimental group during the preneoplastic changes. The experimental group also showed significantly higher expression of hypoxia-inducible factor-1α and vascular endothelial growth factor protein. Our study demonstrated that KC dysfunction and hypoxic environmental changes were the factors influencing preneoplastic change during cholangiocarcinogenesis, and we could non-invasively monitor these changes using CEUS and PAI.

Cholangiocarcinoma (CCA) is a devastating cancer arising from malignant transformation of cholangiocytes which are the epithelial cells lining biliary epithelium[1]. Although the pathophysiology of CCA is poorly understood, it has been noted that the known risk factors, such as liver fluke infections, chronic hepatitis, cirrhosis, and toxins, share the common feature of including cholestatic injury and/or chronic liver inflammation[1–3]. As a result of chronic biliary epithelial injury or inflammation, biliary epithelium is known to be malignantly transformed through a multistep process with epithelial hyperplasia or dysplasia[4]. The precursor lesions, such as biliary intraepithelial neoplasia or intraductal papillary neoplasm of the bile ducts, result from biliary epithelial-cell hyperplasia leading to dysplasia and eventually adenocarcinoma[5,6].

Over the last years a number of animal models of CCA have been developed for a better understanding of the pathophysiology[3]. The bile duct ligation (BDL) causes obstructive cholestatic injury associated with chronic biliary epithelial inflammation and altered Kupffer cell (KC) function which is known as the precursor mechanism of carcinogenesis[7]. N-nitrosodimethylamine (NDMA) is also one of the carcinogens that promotes activation of KCs and causes the DNA structure damage in mice[3]. Previous studies have noted that it has an important role in the development of preneoplastic lesions in that activated KCs release biologically active products including reactive oxygen species and cytokines[8]. Hypoxia, an important microenvironment feature in chronic inflammatory diseases, also likely contributes to carcinogenesis and angiogenesis in hepatic carcinogenesis[9].

[1]Department of Radiology, Seoul National University Hospital, Seoul, Korea. [2]Institute of Radiation Medicine, Seoul National University Hospital, Seoul, Korea. [3]Department of Diagnostic Pathology, Kobe University Graduate School of Medicine, Kobe, Japan. Correspondence and requests for materials should be addressed to J.H.K. (email: jhkim2008@gmail.com)
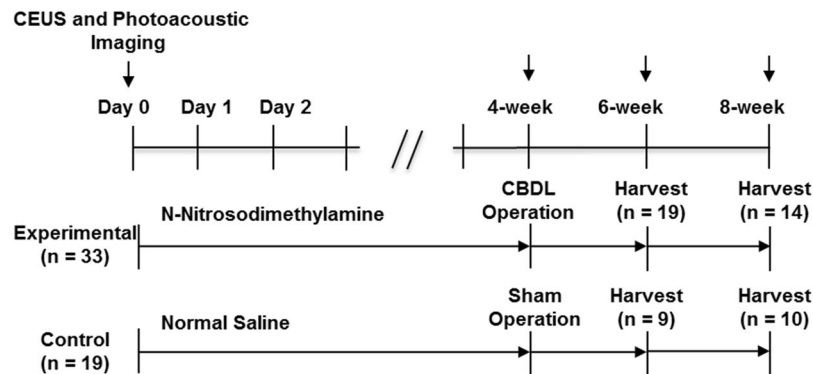
1

Figure 1. Experimental Design. Fifty-two mice were divided randomly into two groups as follows: 19 mice receiving normal saline, and 33 mice receiving *N*- nitrosodimethylamine (NDMA) in drinking water. Four weeks after NDMA administration, common bile duct ligation (CBDL) was performed in the experimental group, whereas sham operation was performed in the control group. The contrast-enhanced ultrasound (CEUS) and photoacoustic imaging were performed at baseline, four-, six- and eight-week follow-up, and then tumor was harvested at six weeks and eight weeks following administration of NDMA or normal saline.

However, there have only been a few studies regarding the image monitoring of the changes in the tissue microenvironment, including the KC function or tissue oxygen saturation (sO_2) in the carcinogenesis. Previously published studies have shown that the function of KCs can be evaluated using contrast-enhanced ultrasound (CEUS) with Sonazoid in rat models[10,11]. Newly developed photoacoustic imaging (PAI) is also a real-time noninvasive and quantitative imaging modality for the study of tissue hypoxia without using a radioisotope or contrast agent[12].

Therefore, our study investigated image monitoring of serial changes of the KC function and hepatic sO_2 using CEUS with Sonazoid and PAI in preneoplastic changes occurring during cholangiocarcinogenesis induced by obstructive cholangitis and NDMA in a mouse model.

Results

A total of 52 mice, including the experimental group (n = 33) and the control group (n = 19), could be assessed for Sonazoid uptake and CD68 expression of KCs (Fig. 1). The degree of sO_2 and expression of hypoxia-inducible factor-1α (HIF-1α) and vascular endothelial growth factor (VEGF) protein in liver parenchyma was also evaluated in each group.

Preneoplastic Changes during Cholangiocarcinogenesis. On histopathologic examination, the livers of the control group showed a normal appearance of hepatocytes, cholangiocytes, and portal triad without evidence of inflammation (Fig. 2A). However, the experimental group showed that there was periductal fibrosis and epithelial hyperplasia in the large bile duct and bile ductular reaction with a periductular inflammatory infiltration around small portal tracts at six weeks (Fig. 2B). At eight weeks, there was an extensive bile ductular reaction with periductular inflammatory infiltrates as well as cystic dilatation with epithelial hyperplasia in the small portal tract. Granulation tissue and bile ductular reaction adjacent to necrosis were noted (Fig. 2C). The large bile ducts also showed epithelial hyperplasia with irregular-shaped ductal architecture and cystic dilatation with enlarged nuclei and slightly distorted polarity (Fig. 2D). Although the biliary epithelial lining was clearly hyperplastic with foci of dysplasia, invasive cancers were not identified (Fig. 2D). These changes were already observed at six week and became more prominent at eight weeks. The histologic findings are summarized in Table 1 as classified into inflammatory changes and preneoplastic changes. The inflammatory changes included zonal necrosis, granulation tissue, periductular infiltration, periductal fibrosis, and cystic dilatation. The preneoplastic changes included epithelial hyperplasia and epithelial dysplasia. Both inflammatory and preneoplastic changes became a more common occurrence as time progressed. At 8-week, the experimental group showed the epithelial hyperplasia (14/14, 100%) and dysplasia (12/14, 85.7%), and these findings were considered to be preneoplastic changes (Table 1).

Changes in Kupffer-phase Echogenicity and the Kupffer Cell Fraction. The bile duct dilatation became increasingly clear from the four-week to the eight-week follow-up in the experimental group. The baseline parenchymal echogenicity on the Kupffer phase of CEUS did not differ significantly between the experimental group and the control group (-30.6 ± 0.9 dB vs. -30.7 ± 1.0 dB, $P = 0.752$). Four weeks after the baseline imaging, the parenchymal echogenicity in the experimental group was slightly increased compared to that of the control group (-29.8 ± 1.3 dB vs. -30.5 ± 0.7 dB, $P = 0.001$). However, the parenchymal echogenicity in the experimental group seen at the six- and eight–week on the Kupffer phase of CEUS, had decreased compared to that of the control group (-35.1 ± 3.8 dB vs. -30.4 ± 0.9 dB and -38.2 ± 4.4 dB vs. -31.2 ± 1.0 dB, all $P < 0.001$). The difference in the parenchymal echogenicity between the experimental and the control group increased from six to eight weeks. (Fig. 3A,B).

The KC fractions in the experimental group according to the CD68 examination were significantly higher than those of the control group at six weeks and eight weeks (24.1 ± 4.7 vs. $12.0 \pm 2.2\%$ and 27.4 ± 7.8 vs. $12.6 \pm 3.6\%$,
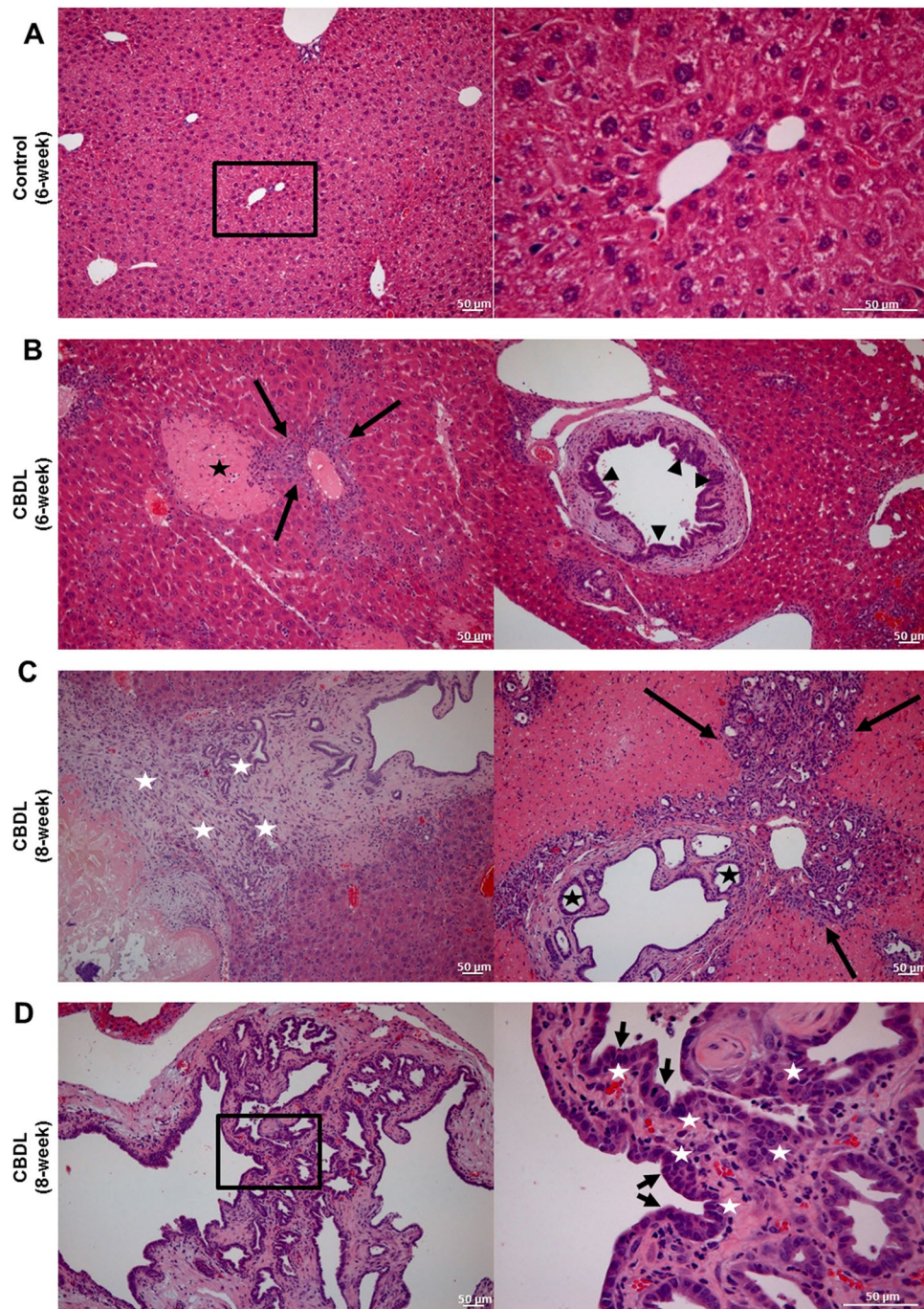
Figure 2. Preneoplastic Changes during Cholangiocarcinogenesis. (**A**) The livers of the control group showed a normal appearance of hepatocytes, cholangiocytes, and portal triad without evidence of inflammation (original magnification; left: ×40 and right: ×200, scale bars = 50 μm). (**B**) The experimental group showed that there was bile ductular reaction with a periductular inflammatory infiltrate (arrows), zonal necrosis (star), and epithelial hyperplasia (arrowheads) at six weeks (original magnification; ×40, scale bars = 50 μm). (**C**) At eight weeks, there was granulation tissue and bile ductular reaction (white stars) adjacent to necrotic area. An extensive bile ductular reaction with a periductular inflammatory infiltrate (arrows), and the cystic dilatation with epithelial hyperplasia (black star) were noted around the small portal tract (original magnification; ×40, scale bars = 50 μm). (**D**) The large bile duct showed that there was biliary epithelial hyperplasia with irregularly shaped ductal architecture (arrow), and the lining epithelium had enlarged nuclei and slightly distorted polarity (white stars) (original magnification; left ×40 and right: ×200, scale bars = 50 μm). These findings was consistent with preneoplastic changes during cholangiocarcinogenesis.

	Experimental Group (n = 33)	
Histologic Findings	6-week (n = 19)	8-week (n = 14)
Inflammatory Changes		
Zonal necrosis	11 (57.9%)	10 (71.4%)
Granulation tissue	3 (15.8%)	11 (78.6%)
Periductular infiltration	18 (94.7%)	14 (100.0%)
Periductal fibrosis	15 (78.9%)	14 (100.0%)
Cystic dilatation	10 (52.6%)	9 (64.3%)
Preneoplastic Changes		
Epithelial hyperplasia	**16 (84.2%)**	**14 (100.0%)**
Epithelial dysplasia	**3 (15.8%)**	**12 (85.7%)**

Table 1. Preneoplastic Changes during Cholangiocarcinogenesis. Note— The table shows the number and percentage of histologic findings in the experimental group. The control group did not show inflammatory change nor preneoplastic change in histologic findings.

all $P < 0.001$). The KC fraction of the experimental group tended to increase slightly from six weeks to eight weeks (Fig. 3C,D).

Changes in Hepatic Oxygen Saturation and Hypoxia-related Protein Expression. We did not find a significant difference between the experimental group and the control group in terms of the baseline sO_2 on PAI ($50.6 \pm 5.3\%$ vs. $49.4 \pm 4.5\%$, $P = 0.263$). However, the sO_2 in the experimental group was lower than that in the control group at four, six, and eight weeks (45.2 ± 4.0 vs. $51.9 \pm 4.4\%$, 43.0 ± 10.2 vs. $49.0 \pm 3.9\%$, and 31.3 ± 7.3 vs. $49.7 \pm 4.0\%$, all $P < 0.001$). The difference in the sO_2 between the experimental group and the control group increased from four to eight weeks (Fig. 4A,B).

To further reveal the induced hypoxic environment during carcinogenesis, we assessed the expression of hypoxia-related protein using Western blot analysis. Even though the experimental group showed higher expression of HIF-1α and VEGF protein than the control group, there was no significant difference at six weeks (0.71 ± 0.29 vs. 0.31 ± 0.01 and 0.44 ± 0.19 vs. 0.16 ± 0.02, $P = 0.302$ and $P = 0.347$). However, the experimental group showed significantly higher expression of HIF-1α and VEGF protein than the control group at eight weeks (1.47 ± 0.48 vs. 0.19 ± 0.08 and 0.96 ± 0.23 vs. 0.33 ± 0.06, $P = 0.019$ and $P < 0.018$) (Fig. 4C–E).

Discussion

Our results showed that KC dysfunction and hypoxic environmental changes were the factors of preneoplastic change during cholangiocarcinogenesis induced by obstructive cholangitis and NDMA in a mouse model, and we could non-invasively monitor these changes using CEUS with Sonazoid and PAI. CEUS with Sonazoid in the experimental group showed that the liver parenchymal echogenicity was reduced, and which indicates that the Sonazoid uptake by KCs was reduced. However, an increase in the number of KC fractions suggested that functionally impaired KCs increased during the preneoplastic change. HIF-1α and VEGF proteins were also expressed in response to hypoxia, while sO_2 of liver parenchyma decreased on PAI during preneoplastic change. Therefore, we determined that KC dysfunction and hypoxic environmental changes were the factors of preneoplastic change during cholangiocarcinogenesis, and we could non-invasively monitor these changes using CEUS and PAI.

Cholangiocarcinogenesis is a multi-step process dependent on an interaction between genetic and environmental factors[1]. The precursor lesions, such as biliary intraepithelial neoplasia and intraductal papillary neoplasm of the bile ducts, are believed to gradually progress to CCA through molecular changes such as alteration of oncogenes and tumor suppressor genes[5,13]. Chronic biliary tract inflammation is known to progress to hyperplasia or dysplasia of bile epithelium, and which pathways are induced by inflammatory mediators or tissue responses and leading to adenocarcinoma[4]. Our experimental group showed that there were zonal necrosis, granulation tissue, periductular infiltration, periductal fibrosis and cystic dilatation, and these findings were considered to be inflammatory changes. At 8-week, the experimental group showed the epithelial hyperplasia (14/14, 100%) and dysplasia (12/14, 85.7%), and these findings were considered to be preneoplastic changes. Our study did not demonstrate the development of CCA arising from the chronic inflammation and NDMA administration. However, we found biliary epithelial hyperplasia with dysplastic cells, which meant the premalignant condition of CCA such as biliary intraepithelial neoplasia (BilIN), in our animal model.

KCs are liver resident macrophages that localize within the lumen of the liver sinusoids and are the first immune cells in the liver that activate an important immune function against chronic inflammation[14]. The results of this activation include the production and secretion of a variety of inflammatory cytokines, reactive oxygen species, and growth regulatory mediators[14]. Although the function of KCs is still controversial in the carcinogenesis process, previous studies have reported that it has an important role in promoting the clonal expansion of preneoplastic cells required for DNA damage and cell growth regulation[8,14–17]. Our study also demonstrated that the number of KCs was increased during preneoplastic change in the experimental group. However, when there was neovascularization during carcinogenesis, normal sinusoids were gradually destroyed and the function of KCs might be changed[18].

Sonazoid is a microbubble with negative charge which has a lipid shell, and these microbubbles are easily phagocytosed by KCs[19]. Recently published data had shown that the changes in KC function induced by cholangitis, could be successfully monitored by CEUS[20]. Therefore, the phagocytic function of KCs can be non-invasively
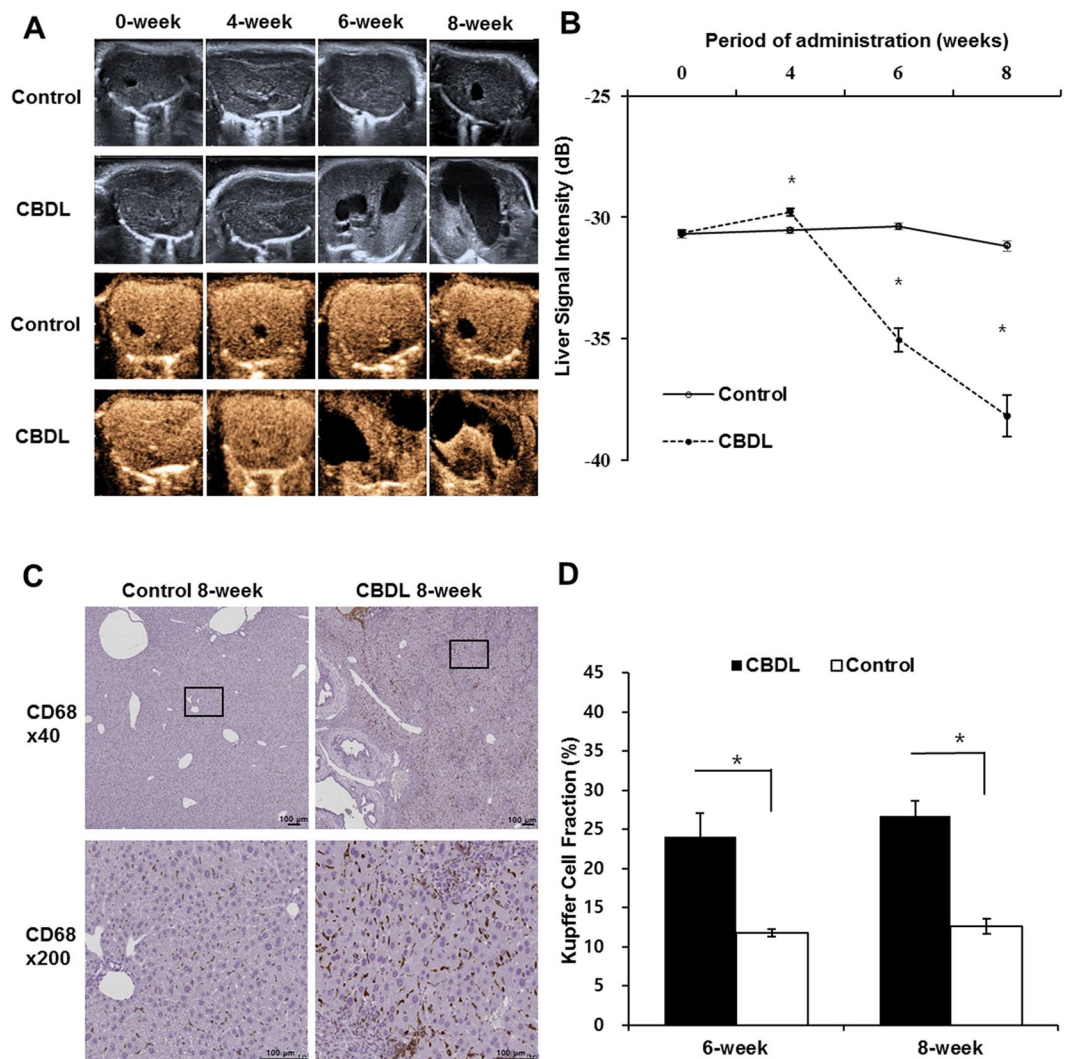
Figure 3. Changes in Kupffer-phase Echogenicity and the Kupffer cell Fraction. **(A)** In the representative case, the bile duct dilatation became increasingly clear from the four-week to eight-week follow-up in the experimental group. The liver parenchymal echogenicity on Kupffer phase by contrast-enhanced ultrasound imaging (CEUS) decreased compared to that of the control group. **(B)** The vertical axis is the signal intensity (dB) and the horizontal axis is the period of *N*-nitrosodimethylamine or normal saline administration. The parenchymal echogenicity in the experimental group at six- and eight-week on the Kupffer phase of CEUS decreased compared to those of the control group (all $P < 0.001$). **(C)** There was significant increase in CD68 count in the experimental group at six- and eight-week specimen ($P < 0.001$) (original magnification; lower power: ×40 and high power: ×200, scale bars = 100 μm). **(D)** The KC fraction of the experimental group tended to increase slightly from six weeks to eight weeks (24.1 ± 4.7 vs. $12.0 \pm 2.2\%$ and 27.4 ± 7.8 vs. $12.6 \pm 3.6\%$). *$P < 0.05$.

monitored in the Kupffer-phase of CEUS, and the reduced contrast effect in the liver parenchyma has been attributed to KC dysfunction[10,11,21]. During non-invasive image monitoring, we found a significant decrease of liver parenchymal enhancement by Sonazoid in the experimental group after six weeks. Despite increased KC numbers, we speculate that Kupffer cells lose their functional ability to take up Sonazoid. Our hypothesis is that reduced phagocytic activity of the KCs is one of the features in the preneoplastic change during cholangiocarcinogenesis.

Moreover, in recent years it has become increasingly evident that hypoxia induced by the development of chronic inflammation causes cholestasis associated with a marked reduction in the expression of hepatobiliary transporters, and also contributes to carcinogenesis in chronic liver injury[9]. Hypoxia has a critical role in carcinogenesis, angiogenesis or tumor progression, and which is mediated by HIF-1α protein[22,23]. Therefore, it is important to investigate the feasibility of hypoxia monitoring and elucidate the involvement of HIF-1α expression during carcinogenesis.

Recent studies have highlighted the usefulness of PAI as a hypoxia monitoring tool in preclinical models[12,24,25]. PAI provides information on sO$_2$ using the absorption characteristics of hemoglobin or deoxy-hemoglobin[26].
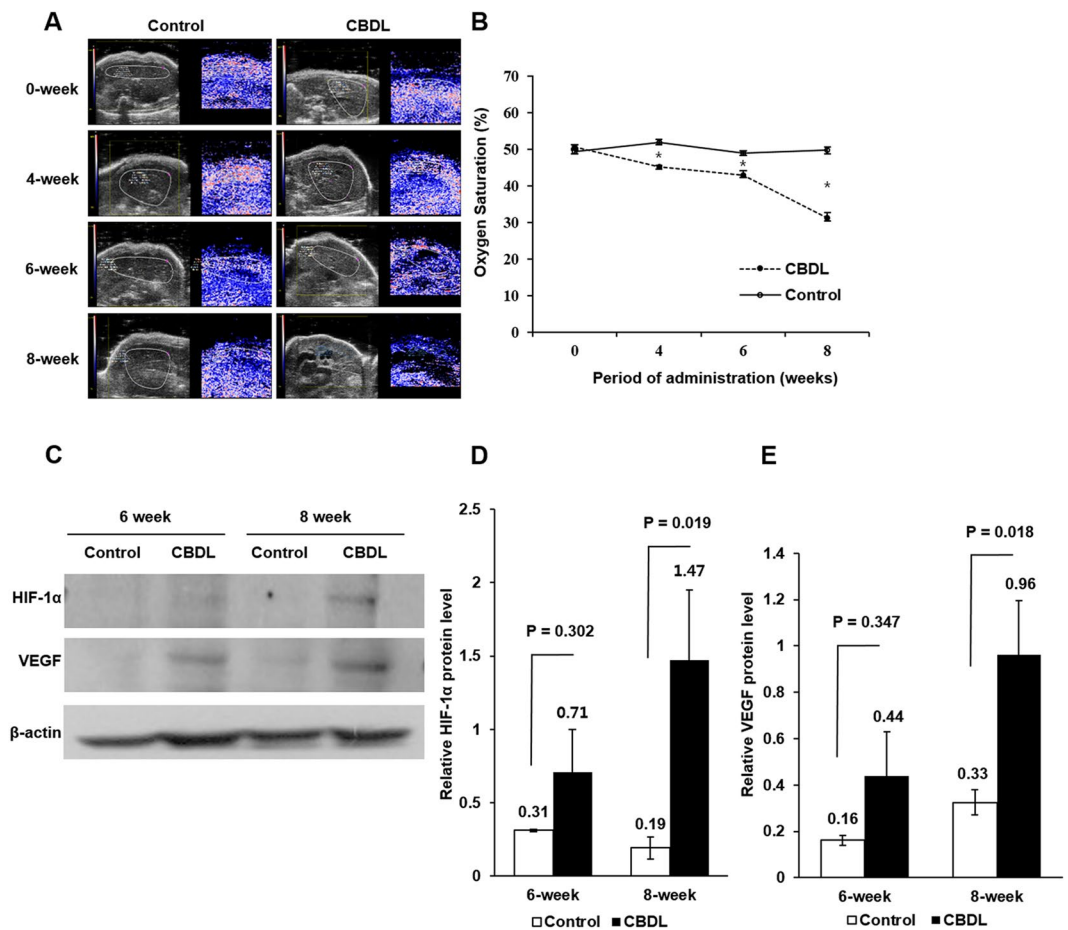
Figure 4. Changes in Hepatic Oxygen Saturation and Hypoxia-related Protein Expression. **(A)** In the representative case, the hepatic oxygen saturation in the experimental group was lower than that in the control group at four, six, and eight weeks (51.6 vs. 54.5%, 48.4 vs. 53.9%, 32.3 vs. 43.2%, and 31.2 vs. 42.9%). **(B)** There was significant decrease of oxygen saturation of liver parenchyma in the experimental group compared to those of control group (45.2 vs. 51.9%, 43.0 vs. 49.0%, and 31.3 vs. 49.7%) at the four, six, and eight weeks, respectively ($P < 0.001$). **(C)** In the Western blot analysis, the experimental group was relatively higher expression of hypoxia-inducible factor-1α (HIF-1α) and vascular endothelial growth factor (VEGF) protein than the control group at eight weeks. The full-length blots with these antibodies were presented in supplementary Figure S1. **(D,E)** The experimental group showed significantly higher expression of HIF-1α and VEGF protein than the control group at eight-week (1.47 ± 0.48 vs. 0.19 ± 0.08 and 0.96 ± 0.23 vs. 0.33 ± 0.06, $P = 0.019$ and $P < 0.018$). *$P < 0.05$.

This method of measuring sO_2 depends on the presence of an endogenous chromophore, ie, hemoglobin, in the target tissue[25]. Lee et al.[20] reported PAI was useful for monitoring the serial change of liver sO_2 in a mouse cholangitis model. Gerling et al.[24] also reported the feasibility of measuring sO_2 in a murine tumor model during tumor development and indicated that sO2 data were associated with hypoxic staining results. In our study, the sO_2 of the experimental group was lower than that of the control group at four, six, and eight weeks, and it could be non-invasively monitored that hypoxia was induced in the preneoplastic change during cholangiocarcinogenesis. One hypothesis is that chronic liver injury could result in an increased resistance to blood flow and oxygen delivery, and thus leading to hypoxia during carcinogenesis and that it is also another feature in the preneoplastic change during cholangiocarcinogenesis. Yang et al.[27] demonstrated that chronic liver injury by BDL transiently increased HIF-1α protein expression during cholestasis-associated carcinogenesis in a mouse model. Tian et al.[23] also reported that overexpression of HIF-1α was emerging as an significant factor in carcinogenesis on the molecular level in CCA. It has been noted that HIF-1α transcriptionally activates VEGF protein, and which is a critical factor for angiogenesis, especially in areas of hypoxia[28]. Our study also demonstrated that the HIF-1α and VEGF expression increased in preneoplastic change during cholangiocarcinogenesis.

As a result of chronic inflammatory changes, biliary epithelium is known to be malignantly transformed through a multistep process with epithelial hyperplasia or dysplasia. Cholangiocarcinogenesis is a broad spectrum that leads to inflammatory changes and preneoplastic changes, and finally cancer development. The environmental changes described in our study was the changes of KCs and hypoxia-inducible factors although BilIN means a microscopic epithelial change. One hypothesis might be addressed regarding the tumor microenvironment

in our results. CCA is characterized by a prominent desmoplastic stroma such as cancer-associated fibroblasts, tumor-associated macrophages and vascular cells. These factors undergoes profound changes in its composition and function during cholangiocarcinogenesis[29]. Therefore, our results could support the altered function of sinusoidal macrophages and dynamic changes of carcinogenesis-associated neovascularization. This study suggests that CEUS and PAI may be useful in monitoring carcinogenesis process to precancerous lesions even if cholangiocarcinogenesis is a broad spectrum that leads to inflammation, periductal fibrosis, precancerous dysplasia, and cancer development.

Our study has several limitations. First, the function of KC in our study was indirectly assessed by the Sonazoid phagocytosis ability of KC. However, KC is activated under pathological conditions and then functions in various ways through differentiation into M1 or M2 macrophages[14]. Previous animal studies have been performed only to demonstrate changes in phagocytic function of KCs in a rat model of nonalcoholic steatohepatitis[11,30]. Few studies have documented functional changes in KCs except for CEUS. In this study, we used an ultrasound contrast agent, which is easily phagocytosed by KCs. CEUS can assess KC phagocytic activity using the Kupffer-specific contrast agent[10,11]. The effect of ultrasound contrast agent phagocytosis by KCs can provide a stable, late-stage CEUS image called "Kupffer-phase" imaging[19]. A potential benefit of this CEUS imaging is that the quantitative changes in contrast enhancement values would provide data that reflects *in vivo* physiologic function of KC. Although we used the CEUS imaging that reflects the physiologic function of KC, further studies are needed to understand the implications of KC function changes during preneoplastic changes in liver parenchyma. In future studies, the phagocytosis by differentiated KCs during carcinogenesis needs to be directly evaluated through molecular work.

Second, some studies have used the pimonidazole injection model to assess the development of hypoxia during chronic liver injury or carcinogenesis[9,24,31]. However, we focused on non-invasive image monitoring of the hypoxic development in the carcinogenesis process. If pimonidazole can directly demonstrate the area of hypoxia, it could be direct evidence of hypoxia in the carcinogenesis process. On the other hand, there were a few studies that demonstrated the possibility of imaging monitoring in animal models using invasive needle or radioisotope in terms of hypoxia monitoring[32,33]. Recent interest in tumor hypoxic conditions has shifted to the area of diagnostic imaging due to the rapid development of diagnostic methods. PAI is a real-time, non-invasive and quantitative imaging method for hypoxia monitoring[12]. We were able to non-invasively monitor *in vivo* quantitative data of sO_2 during preneoplastic changes in liver parenchyma through PAI without using radioisotope. PAI can provide quantitative information by measuring tissue sO_2 using the optical absorption differences between oxygenated and deoxygenated hemoglobin[24,25]. However, the depth limitation of photoacoustic signals (ie, optical enabled penetration of 8 mm at excitation wavelength between 750 nm and 850 nm) still severely limits the clinical application of PAI[34]. Therefore, additional technical advances are needed to improve the detection and visibility of photoacoustic signals emitted from deeply located lesion.

Finally, our study could not establish the development of CCA arising from the chronic inflammation and NDMA administration. However, we found biliary epithelial hyperplasia with dysplastic cells, which meant the premalignant condition of CCA such as BilIN, in our animal model. Based on the degree of cellular and structural atypia, BilIN can be classified into three grades indicating low-grade dysplasia, high-grade dysplasia, and carcinoma *in situ* respectively[4]. The environmental changes described in our study was the changes of KCs and hypoxia-inducible factor, and our hypothesis might be addressed regarding the tumor microenvironment.

In conclusion, obstructive cholangitis and continued administration of NDMA promote preneoplastic changes during cholangiocarcinogenesis in mouse models. Our study demonstrated that KC dysfunction and hypoxic environmental changes were the causes of preneoplastic change and that we could non-invasively monitor these changes using CEUS with Sonazoid and PAI.

Methods

This study was approved by our Institutional Animal Care and Use Committee (IACUC; No. 13-0369-C3A0) and was performed in accordance with the Guide for our IACUC and National Institute of Health Guide for the Care and Use of Laboratory Animals.

Experimental Protocol.   Six-week–old, male, BALB/c nude mice weighing 25 g were randomized into one of two groups as follows: (1) the experimental group (n = 33); and (2) the control group (n = 19). In the experimental group, NDMA was administered at a concentration of 12.5 ppm in drinking water for eight weeks, and only normal saline was administered in the control group.

Four weeks after the administration, BDL was performed in the experimental group, and the control group was made by sham operation. After intraperitoneal general anesthesia with 5 mg/kg zolazepam (Zoletil, Virbac, Carros, France) and xylazine hydrochloride (Rompun 2%, Bayer Korea, Seoul, Korea), the skin and peritoneum were incised along the midline of the animal. After lifting the entire liver, the common bile duct (CBD) before draining into the duodenum was gently isolated with moistened cotton gauze and microdissecting forceps. The distal CBD was ligated using 7-0 Prolene (Ethicon, Somerville, NJ) and the peritoneum was closed with Prolene.

CEUS and PAI were performed baseline, four-, six- and eight-weeks follow-up examinations following administration of NDMA or normal saline in order to observe bile duct dilatation, contrast agent uptake by KC, and changes in sO_2 of liver parenchyma. Histopathologic examination was performed at six weeks (n = 28) and eight weeks (n = 24) (Fig. 1).

Contrast-enhanced Ultrasound Examination.   The CEUS examination was performed by a radiologist (J.H.K.) with 17 years of clinical experience performing liver ultrasound. The Aplio-500 ultrasound equipment (Toshiba Medical Systems Corp., Ototara, Japan) and a center frequency, 12-MHz linear transducer were used

as the following parameters for B-mode imaging: a dynamic range of 65; a mechanical index of 0.9; a gain of 95; and a field-of-view depth of 1.5 cm. Ultrasonography for examining morphological features, including biliary dilatation, was performed in the B-mode.

After determining the optimal plane covering the wide range of liver parenchyma, ultrasound contrast agent Sonazoid (gaseous perflubutane; GE Healthcare, Waukesha, WI, USA) was intravenously injected at a dose of 3 μl/kg and was flushed with 0.2 mL saline. After 10 minutes of contrast agent injection, image acquisition was performed for 10 seconds and which corresponds to the Kupffer-phase in CEUS[19,35,36]. Shunichi et al.[36] defined the Kupffer-phase images from the time point at which the liver parenchyma was enhanced starting 10 min after Sonazoid injection. Sontum et al.[35] and Yanagisawa et al.[19] had performed in vitro and in vivo experiments with Kupffer-phase imaging at 10 min after the injection of Sonazoid, when the hepatic parenchyma appeared homogeneously bright by physiochemical characteristics of Sonazoid. In addition, Miyata et al.[11] defined the Kupffer-phase as 10 min after the injection of Sonazoid in a rat experiment, and Sugimoto et al.[37] also observed the Kupffer-phase images in a similar method in a clinical study. The main advantage of Sonazoid is that it facilitates stable Kupffer-phase imaging with real-time visualization[38].

CEUS images were acquired using a contrast harmonic image mode (CHI; Toshiba Medical Systems, Japan) with the following parameters: a transmission frequency of 12-MHz; a frame rate of 8 Hz; a dynamic range of 40; a mechanical index of 0.20; a gain of 73; and a depth of 1.5 cm. The evaluation of echogenicity by the contrast agent of all of the recorded raw data was performed using dedicated software (CHI-Q software, Toshiba Medical Systems, Japan). The average parenchymal echogenicity value was obtained by manually drawing the ROI three times while avoiding large blood vessels in the liver parenchyma. The serial change of liver parenchymal echogenicity in the Kupffer-phase imaging was measured at baseline, four-, six-, and eight-week follow-up examinations.

High-resolution, Photoacoustic Ultrasound Examination.

The examination of sO_2 was performed by a radiologist (J.H.K.) with four years of PAI experience. A commercially available, high-resolution, photoacoustic imaging system (VisualSonics, Toronto, Ontario, Canada) and a central frequency, 21-MHz, LZ-250 PA linear transducer were used with the following parameters: a depth of 20.0 mm; a width of 23.04 mm; and a wavelength of 750/850 nm.

For the assessment of sO_2, after placing the transducer at the target lobe of the liver, the liver was investigated by PAI in the OxyHemo-Mode so that the laser was fired with dual wavelengths of 750 and 850 nm during room air breathing[24]. As the binding of oxygen to hemoglobin alters its absorption spectrum according to different wavelengths, comparing the photoacoustic signal at 750 and 850 nm allowed for determination of the percent of oxygenation levels within the liver from the parametric maps of the sO_2[24,25].

In the sO_2 parametric map of each target lobe, the ROI was drawn three times in order to obtain the average value. Serial change of liver sO_2 in the PAI was measured at baseline and at the four-, six-, and eight-week follow-up examinations.

Histologic Analysis.

All of the mice were serially sacrificed at six weeks and eight weeks following administration of NDMA or normal saline. Among all of the mice (n = 52), there were 28 available specimens at six weeks and 24 specimens at eight weeks.

The specimens were fixed using 10% neutral-buffered formalin, embedded in paraffin, and cut into 4-um sections. Each section was stained with Harris' hematoxylin solution and eosin Y (H&E) (Sigma, St. Louis, MO, USA) so that a pathologist (Y.Z.) could assess bile duct changes. Microscopic changes were evaluated according to the standard of human biliary pathology. Bile ductular reaction was defined as an increased number of bile ductules at the interface between portal tracts and the liver parenchyma. Biliary epithelial hyperplasia was micropapillary or pseudopapillary proliferation of non-dysplastic epithelial cells, while dysplasia was defined as the presence of atypical cellular changes including the irregular nuclear membrane, hyperchromasia, and loss of cellular polarity. The latter dysplastic changes corresponded to biliary intraepithelial neoplasia in human. The presence or absence of periductal inflammation and fibrosis was also examined. Histological evidence of stromal invasion was a requisite for the diagnosis of cholangiocarcinomas.

CD68 immunohistochemical staining was also performed using rabbit polyclonal antibody to CD68 (ab125212, 1:500 Abcam, Cambridge, UK) as the primary antibody and horseradish peroxidase (HRP)-labelled, polymer anti-rabbit antibody (K4003, Dako) as the secondary antibody.

CD68-stained images were analyzed using ImageJ 1.44 software (Wayne Rasband, NIH, MD, USA). Five hot spots (areas of higher CD68, positive brown staining compared with the rest of the tissue) were randomly selected at low magnification (×40) and the number of CD68-stained KCs was measured at high magnification (×200, 0.7386 mm^2) in the hot spots. Finally, the fraction of the CD68-stained KCs from each slice was calculated five times and was then averaged.

Western Blot Analysis.

To verify the expression of HIF-1α and VEGF proteins, the total protein in the tissue samples was homogenized and lysed with ice-cold RIPA buffer (50 mmol/L Tris, 150 mmol/L NaCl, 1% NP40, protease, and phosphatase inhibitor). Protein extracts were separated using 10% polyacrylamide gel and were electro-transferred to nitrocellulose membranes. After blocking with 5% milk in TBST buffer (10 mmol/L Tris-HCl, 150 mmol/L NaCl, and 0.05% Tween-20), the membranes were probed with primary antibodies: HIF-1α (NB100-449, Novus Biologicals, Littleton, CO, USA); VEGF (ab46154, Abcam, CA, MA, USA); and actin (A2066, Sigma-Aldrich, St. Louis, MO, USA), followed by incubation with HRP-conjugated secondary antibody (T6778, Sigma-Aldrich, St. Louis, MO, USA). The target bands were visualized using enhanced chemiluminescence reagent (Amersham Biosciences), and the band images were quantified using ImageJ software (National Institutes of Health, Bethesda, MD, USA).

Statistical Analysis. All statistical analyses were performed using SPSS version 21.0 (SPSS, Chicago, IL, USA). Results with a P value less than 0.05 were considered statistically significant. The parenchymal echogenicity and sO_2 were assessed using the unpaired t-test to compare the significant differences between the experimental group and the control group. The unpaired t-test was also used to compare the CD68 count and the protein expression level (HIF-1α and VEGF) in each group.

References

1. Khan, S. A., Thomas, H. C., Davidson, B. R. & Taylor-Robinson, S. D. Cholangiocarcinoma. *Lancet* **366**, 1303–1314 (2005).
2. Blechacz, B. & Gores, G. J. Cholangiocarcinoma: advances in pathogenesis, diagnosis, and treatment. *Hepatology* **48**, 308–321 (2008).
3. De Minicis, S. *et al*. Liver carcinogenesis: rodent models of hepatocarcinoma and cholangiocarcinoma. *Dig Liver Dis* **45**, 450–459 (2013).
4. Sibulesky, L., Nguyen, J. & Patel, T. Preneoplastic conditions underlying bile duct cancer. *Langenbecks Arch Surg* **397**, 861–867 (2012).
5. Lewis, J. T., Talwalkar, J. A., Rosen, C. B., Smyrk, T. C. & Abraham, S. C. Precancerous Bile Duct Pathology in End-stage Primary Sclerosing Cholangitis, With and Without Cholangiocarcinoma. *Am J Surg Pathol* **34**, 27–34 (2010).
6. Nakanuma, Y. A novel approach to biliary tract pathology based on similarities to pancreatic counterparts: Is the biliary tract an incomplete pancreas? *Pathology International* **60**, 419–429 (2010).
7. Liedtke, C. *et al*. Experimental liver fibrosis research: update on animal models, legal issues and translational aspects. *Fibrogenesis Tissue Repair* **6**, 19 (2013).
8. Roberts, R. A. *et al*. Role of the Kupffer cell in mediating hepatic toxicity and carcinogenesis. *Toxicol Sci* **96**, 2–15 (2007).
9. Rosmorduc, O. & Housset, C. Hypoxia: A Link between Fibrogenesis, Angiogenesis, and Carcinogenesis in Liver Disease. *Semin Liver Dis* **30**, 258–270 (2010).
10. Tsujimoto, T. *et al*. Decreased phagocytic activity of Kupffer cells in a rat nonalcoholic steatohepatitis model. *World J Gastroenterol* **14**, 6036–6043 (2008).
11. Miyata, Y., Miyahara, T. & Moriyasu, F. Decreased accumulation of ultrasound contrast in the liver of nonalcoholic steatohepatitis rat model. *World J Gastroenterol* **17**, 4191–4198 (2011).
12. Raes, F. *et al*. High Resolution Ultrasound and Photoacoustic Imaging of Orthotopic Lung Cancer in Mice: New Perspectives for Onco-Pharmacology. *Plos One* **11**, e0153532 (2016).
13. Bickenbach, K., Galka, E. & Roggin, K. K. Molecular mechanisms of cholangiocarcinogenesis: are biliary intraepithelial neoplasia and intraductal papillary neoplasms of the bile duct precursors to cholangiocarcinoma? *Surg Oncol Clin N Am* **18**, 215–224 (2009).
14. Nguyen-Lefebvre, A. T. & Horuzsko, A. Kupffer Cell Metabolism and Function. J *Enzymol Metab* 1 (2015).
15. Peters, J. M., Cheung, C. & Gonzalez, F. J. Peroxisome proliferator-activated receptor-alpha and liver cancer: where do we stand? *J Mol Med (Berl)* **83**, 774–785 (2005).
16. Wu, J. *et al*. The proinflammatory myeloid cell receptor TREM-1 controls Kupffer cell activation and development of hepatocellular carcinoma. *Cancer Res* **72**, 3977–3986 (2012).
17. Gul, N. *et al*. Macrophages eliminate circulating tumor cells after monoclonal antibody therapy. *J Clin Invest* **124**, 812–823 (2014).
18. Inoue, T. *et al*. Kupffer phase image of Sonazoid-enhanced US is useful in predicting a hypervascularization of non-hypervascular hypointense hepatic lesions detected on Gd-EOB-DTPA-enhanced MRI: a multicenter retrospective study. *J Gastroenterol* **51** (2016).
19. Yanagisawa, K., Moriyasu, F., Miyahara, T., Yuki, M. & Iijima, H. Phagocytosis of ultrasound contrast agent microbubbles by Kupffer cells. *Ultrasound Med Biol* **33**, 318–325 (2007).
20. Lee, S., Kim, J. H., Lee, J. H. & Choi, S. Y. Image Monitoring of the Impaired Phagocytic Activity of Kupffer Cells and Liver Oxygen Saturation in a Mouse Cholangitis Model Using Contrast-Enhanced Ultrasound Imaging and Photoacoustic Imaging. *Ultrasound Med Biol* **43**, 2461–2468 (2017).
21. Iijima, H. *et al*. Decrease in accumulation of ultrasound contrast microbubbles in non-alcoholic steatohepatitis. *Hepatol Res* **37**, 722–730 (2007).
22. Lee, J. W., Bae, S. H., Jeong, J. W., Kim, S. H. & Kim, K. W. Hypoxia-inducible factor (HIF-1)alpha: its protein stability and biological functions. *Exp Mol Med* **36**, 1–12 (2004).
23. Tian, Q. *et al*. Overexpression of hypoxia-inducible factor 1 alpha induces migration and invasion through Notch signaling. *International Journal of Oncology* **47**, 728–738 (2015).
24. Gerling, M. *et al*. Real-time assessment of tissue hypoxia *in vivo* with combined photoacoustics and high-frequency ultrasound. *Theranostics* **4**, 604–613 (2014).
25. Rich, L. J. & Seshadri, M. Photoacoustic imaging of vascular hemodynamics: validation with blood oxygenation level-dependent MR imaging. *Radiology* **275**, 110–118 (2015).
26. Laufer, J., Delpy, D., Elwell, C. & Beard, P. Quantitative spatially resolved measurement of tissue chromophore concentrations using photoacoustic spectroscopy: application to the measurement of blood oxygenation and haemoglobin concentration. *Phys Med Biol* **52**, 141–168 (2007).
27. Yang, H. *et al*. A mouse model of cholestasis-associated cholangiocarcinoma and transcription factors involved in progression. *Gastroenterology* **141**(378–388), 388 e371–374 (2011).
28. Josko, J., Gwozdz, B., Jedrzejowska-Szypulka, H. & Hendryk, S. Vascular endothelial growth factor (VEGF) and its effect on angiogenesis. *Med Sci Monit* **6**, 1047–1052 (2000).
29. Banales, J. M. *et al*. Expert consensus document: Cholangiocarcinoma: current knowledge and future perspectives consensus statement from the European Network for the Study of Cholangiocarcinoma (ENS-CCA). *Nat Rev Gastroenterol Hepatol* **13**, 261–280 (2016).
30. Yoshikawa, S. *et al*. Crucial role of impaired Kupffer cell phagocytosis on the decreased Sonazoid-enhanced echogenicity in a liver of a nonalchoholic steatohepatitis rat model. *Hepatol Res* **40**, 823–831 (2010).
31. Moon, J. O., Welch, T. P., Gonzalez, F. J. & Copple, B. L. Reduced liver fibrosis in hypoxia-inducible factor-1alpha-deficient mice. *Am J Physiol Gastrointest Liver Physiol* **296**, G582–592 (2009).
32. Yip, C., Blower, P. J., Goh, V., Landau, D. B. & Cook, G. J. Molecular imaging of hypoxia in non-small-cell lung cancer. *Eur J Nucl Med Mol Imaging* **42**, 956–976 (2015).
33. Fatema, C. N. *et al*. Dual tracer evaluation of dynamic changes in intratumoral hypoxic and proliferative states after radiotherapy of human head and neck cancer xenografts using radiolabeled FMISO and FLT. *Bmc Cancer* **14**, 692 (2014).
34. Beard, P. Biomedical photoacoustic imaging. *Interface Focus* **1**, 602–631 (2011).
35. Sontum, P. C. Physicochemical characteristics of Sonazoid (TM), a new contrast agent for ultrasound imaging. *Ultrasound in Medicine and Biology* **34**, 824–833 (2008).
36. Shunichi, S., Hiroko, I., Fuminori, M. & Waki, H. Definition of Contrast Enhancement Phases of the Liver Using a Perfluoro-Based Microbubble Agent, Perflubutane Microbubbles. *Ultrasound in Medicine and Biology* **35**, 1819–1827 (2009).

37. Sugimoto, K. *et al.* Comparison of Kupffer-phase Sonazoid-enhanced sonography and hepatobiliary-phase gadoxetic acid-enhanced magnetic resonance imaging of hepatocellular carcinoma and correlation with histologic grading. *J Ultrasound Med* **31**, 529–538 (2012).
38. Miyazaki, M. *et al.* Contrast-enhanced ultrasonography using Sonazoid to evaluate changes in hepatic hemodynamics in acute liver injury. *J Gastroen Hepatol* **26**, 1749–1756 (2011).

Acknowledgements

Author Contributions

S.L., design, collection and assembly of data, data analysis and interpretation, manuscript writing; J.H.K., conception and design, data analysis and interpretation, financial support, manuscript writing; J.H.L., collection and assembly of data, data analysis and interpretation; Y.Z., data analysis and interpretation; J.K.H., conception and design, financial support.

Additional Information

Competing Interests: The authors declare that they have no competing interests.

Publisher's note: Springer Nature remains neutral with regard to jurisdictional claims in published maps and institutional affiliations.